This is the accepted manuscript made available via CHORUS. The article has been published as:

Engineering interfacial charge transfer through modulation doping for 2D electronics

Raagya Arora, Ariel R. Barr, Daniel T. Larson, Michele Pizzochero, and Efthimios Kaxiras

Phys. Rev. Materials **9**, L021601 — Published 18 February 2025

DOI: 10.1103/PhysRevMaterials.9.L021601

Engineering Interfacial Charge Transfer through Modulation Doping for 2D Electronics

Raagya Arora,[1,*] Ariel R. Barr,[2] Daniel T. Larson,[3] Michele Pizzochero,[4,1] and Efthimios Kaxiras[3,1,†]

[1] *John A. Paulson School of Engineering and Applied Sciences, Harvard University, Cambridge, Massachusetts 02138, United States*
[2] *Department of Materials Science & Engineering, Massachusetts Institute of Technology, Cambridge, Massachusetts 02139, United States*
[3] *Department of Physics, Harvard University, Cambridge, Massachusetts 02138, United States*
[4] *Department of Physics, University of Bath, Bath BA2 7AY, United Kingdom*

(Dated: February 6, 2025)

Two-dimensional (2D) semiconductors are likely to dominate next-generation electronics due to their advantages in compactness and low power consumption. However, challenges such as high contact resistance and inefficient doping hinder their applicability. Here, we investigate work-function-mediated charge transfer (modulation doping) as a pathway for achieving high-performance p-type 2D transistors. Focusing on type-III band alignment, we explore the doping capabilities of 27 candidate materials, including transition metal oxides, oxyhalides, and α-$RuCl_3$, on channel materials such as transition metal dichalcogenides (TMDs) and group-III nitrides. Our extensive first-principles density functional theory (DFT) reveal p-type doping capabilities of high electron affinity materials, including α-$RuCl_3$, MoO_3, and V_2O_5 . We predict significant reductions in contact resistance and enhanced channel mobility through efficient hole transfer without introducing detrimental defects. We analyze transistor geometries and identify promising material combinations beyond the current focus on WSe_2 doping, suggesting new avenues for hBN, AlN, GaN, and MoS_2. This comprehensive investigation provides a roadmap for developing high-performance p-type monolayer transistors toward the realization of 2D electronics.

I. INTRODUCTION

Layered two-dimensional (2D) semiconductors have attracted attention for their potential to revolutionize electronic devices through miniaturization. The 2D materials family encompasses diverse behavior, including semi-metallic graphene, semiconducting transition metal dichalcogenides (TMDs) and black phosphorus (BP), and insulating hexagonal boron nitride (hBN) [1, 2]. These materials exhibit exceptional electronic and optical properties, making them highly promising candidates for applications in field-effect transistors (FETs), photovoltaic cells, photodetectors, spintronics, sensors, and flexible electronics [3–7].

Despite extensive research demonstrating the superior performance of 2D material-based nanodevices over bulk semiconductors, significant challenges still need to be overcome to achieve practical technological advancements. Two crucial aspects relevant to our study are: (i) the electrical contact between semiconductors and metal electrodes, which governs the charge carrier injection from metal to the 2D channel; and (ii) the doping of the semiconductor layers, which controls the carrier concentration [5].

The first issue, high contact resistance, hampers circuit operation, leading to slower performance, unnecessary heat generation, a reduced on-off ratio, and increased power consumption. When a semiconductor is heavily doped near the metal contact, the increased carrier concentration reduces the width of the depletion region at the interface. This effectively thins the Schottky barrier, facilitating carrier transport through enhanced tunneling. Consequently, contact resistance is lowered, and control over the electrical conduction within the channel layer is improved. However, due to their atomically thin nature, 2D materials do not favor substitutional doping techniques such as ion implantation, which involves bombardment with impurities, because it tends to reduce carrier mobility. Progress in alternative doping techniques, such as electrostatic gating, is still limited by issues like electrical breakdown or the need for sophisticated device fabrication [8]. While advancement of n-type contacts is progressing, research into reliable and low-resistance p-type contacts is somewhat lagging.[9–11]

In what concerns the second issue, adjusting the type and concentration of charge carriers to manipulate electrical conduction has been a fundamental capability driving the progress of electronics and optoelectronics [12, 13]. FETs made from 2D materials generally suffer from reduced carrier mobility, which has been recognized as a major limiting factor in harnessing the full potential of these materials for next-generation nanoelectronics. This limitation can be due to factors like scattering from defects, impurities, or interactions with the substrate the 2D material is placed on. To address both limitations of contact resistance and low carrier concentration, various doping techniques have been explored [12–14].

Maintaining the structural integrity of 2D materials during doping is crucial, as defects can negatively af-

* raagya@g.harvard.edu
† kaxiras@g.harvard.edu

fect the carrier mobility. Effective doping should enhance both carrier density and mobility. In the present study we propose several options for layer combinations that can effectively p-dope 2D channel materials through work-function-mediated interlayer charge transfer [15]. This method, also referred to as "modulation doping" or "remote charge transfer doping", involves providing additional carriers through a separate proximal layer [16–18]. Instead of introducing defects into the 2D channel material, the channel forms a heterostructure with materials possessing extreme work functions, favoring band alignment such that the layer donates electrons or holes to the channel layer, thereby allowing modulation of the channel material's conductivity. This strategy is also called surface transfer doping (STD) since doping is achieved by electron exchange at the interface between the channel surface and a solid dopant [19]. This method bypasses surface treatments and metal evaporation, simplifying p-type doping in 2D semiconductors.

Examples of transistor geometries that favor reductions in contact resistance and/or improved channel mobility, high carrier density are shown in Fig. 1. Using first-principles calculations, we assess the hole transfer capabilities of transition metal oxide films and α-$RuCl_3$, demonstrating robust p-type doping of the channel material, with potential for improving both contact resistance and carrier concentration. We present a list of favorable layer combinations that exhibit charge transfer and emphasize the electron acceptor properties underlining their capacity to reduce contact resistance and enhance channel mobility.

II. RESULTS AND DISCUSSION

We envision devices where the 2D channel is a hexagonal group III nitride or TMD. Hexagonal 2D materials such as hBN and its analogs (hAlN, hGaN) offer exceptional electronic, optical, and thermoelectric properties, along with high mechanical strength. Achieving reliable n-type or p-type doping in these materials has proven to be challenging [20]. Similarly, TMDs have garnered significant attention due to their exceptional properties, including high carrier mobilities, large bandgaps, and atomic thickness [21]. Creating electrical contacts to monolayer TMDs is hindered by the common challenges associated with semiconductor contacts, including Schottky barrier formation and Fermi-level pinning [9].

In order to dope those 2D channels, materials with high work functions like α-$RuCl_3$ have aroused interest for their capacity to function as a charge transfer layer in FET geometries like those schematically shown in Fig. 1. Studies have explored surface charge-transfer doping of 2D WSe_2, achieving superior electrical performance, including a hole density of 4×10^{13} cm^{-2} and a hole mobility exceeding 200 cm^2/Vs [3]. Such levels of doping are challenging to achieve with conventional electrostatic gating due to dielectric breakdown. Oxide materials such as MoO_3 and V_2O_5 are also promising candidates for the STD process [22, 23]. Notably, MoO_3's exceptionally high work function has led to its widespread adoption as an effective anode buffer layer, significantly enhancing hole injection and extraction in organic electronic devices [24, 25]. Moreover, MoO_3 functions as a bulk p-type dopant for organic wide-band-gap materials [26, 27].

The ionization potential (IP) and electron affinity (EA) of a semiconductor or insulator provide crucial insights into their electronic behavior, indicating the ease with which an electron can be released or accepted, respectively. These properties are defined by the energy levels of the valence band maximum (VBM) and conduction band minimum (CBM) relative to the vacuum level (E_{vac}), namely: $E_{IP} = E_{vac} - E_{VBM}$ and $E_{EA} = E_{vac} - E_{CBM}$. Understanding the relative positions of these energy levels across different materials, known as band alignment, is of central importance for the design of devices that effectively utilize interfacial and surface-related phenomena.

We focus on heterojunctions with type-III band alignment, also known as a broken gap, characterized by a substantial energy offset such that the CBM of one material lies below the VBM of an adjacent material, resulting in a direct overlap between those two band manifolds. This broken-gap configuration induces spontaneous charge transfer. The applicability of type-III band alignment in advanced devices is particularly beneficial for tunneling-based applications, such as tunneling field-effect transistors, infrared detectors, and photodetectors, where low-power operation and efficient charge transfer are essential [28–31]. The heterostructure formed from WSe_2 and α-$RuCl_3$ offers a concrete example of how type-III band alignment works: the CBM of α-$RuCl_3$ is positioned below the VBM of WSe_2, facilitating spontaneous charge transfer from WSe_2 to α-$RuCl_3$ and resulting in a heavily p-doped WSe_2 layer [3, 32].

We employed first-principles density functional theory (DFT) calculations using the HSE06 functional to determine E_{IP} and E_{EA} for 21 binary oxides, 2 MXO (M: Metal, X: Halide, O: Oxygen), 3 A_2BO_4 layers (A: Ba/Ca/Sr, B: Ti, O: Oxygen), and α-$RuCl_3$. This computational approach allows us to rigorously analyze the band alignment of these materials and identify optimal candidates for effective p-type doping of TMDs and group III nitride materials (for details see Supplementary Information, (see in Supplementary Information [61] see also references [62-70] therein)). The essential criterion for selecting promising materials is that they must possess a sufficiently high work function for hole doping or a sufficiently low work function for electron doping. Devices built from 2D materials with appropriately aligned energy levels will have enhanced performance due to improved charge carrier injection and reduced contact resistance.

Incorporating a modulation doping layer can enhance two critical properties of FETs. Fig. 1(a) shows the charge-transfer architecture, wherein a van der Waals

(vdW) electron acceptor material, such as those studied here, is placed in contact with the entire 2D channel. This approach alters the doping state of the 2D channel, resulting in higher carrier mobility compared to intrinsically doped TMD-based transistors [33]. Modifications to this geometry, incorporating a vdW hBN spacer layer between the charge transfer layer and the 2D channel, offer a compelling route to enhance device performance by enabling effective confinement of doped carriers. Recent experimental strategies have successfully demonstrated the efficacy of inserting vdW hBN spacer layers in similar device architectures [16].

Fig. 1(b) presents an alternative device architecture incorporating charge transfer layers to selectively dope the contact regions. Within this structure, the contact metal largely dictates the Fermi level within the 2D channel. Consequently, the electron Schottky barrier height (SBH) corresponds to the energy difference between the Fermi level and the CBM, while the hole SBH is defined as the energy separation between the Fermi level and the VBM, as illustrated in the right panel of Fig. 1(a). By modifying the modulation doping layer, we can effectively tune the Fermi level position across a significant portion of the 2D semiconductor's band gap. This tunability allows for a reduction in the SBH for either hole or electron doping, as shown in the right panel of Fig. 1(b), highlighting the potential for optimizing device performance through modulation doping [33]. This strategy aligns with recent work by Jordan Pack *et al.* [32], who demonstrated that α-$RuCl_3$ can exclusively dope the contact region of an hBN-encapsulated monolayer WSe_2 device. While the experimental availability of these materials makes the creation of such heterostructures attainable, their (electro-)chemical reactivity necessitates meticulous optimization.

To understand better the microscopic details of charge transfer, we calculated the charge density difference for specific pairings of channel materials and doping layers. The charge density difference, $\Delta\rho$, is defined as:

$$\Delta\rho = \rho_{A/B} - \rho_A - \rho_B \quad (1)$$

where $\rho_{A/B}$, ρ_A, and ρ_B denote the charge densities of the combined heterostructure, the isolated layer A, and the isolated layer B, respectively. We show two representative channel material/doping layer pairs in Fig. 2: (a) $MoSe_2$ with α-$RuCl_3$, and (b) WSe_2 with α-MoO_3. To elucidate the charge rearrangement and interlayer coupling mechanism in these heterostructures, we calculated the plane-averaged charge density difference along the z-axis: yellow isosurfaces of the charge density difference indicate charge accumulation (excess electrons), while cyan isosurfaces indicate charge depletion (excess holes). As is clear from the results shown in Fig. 2, charge depletion predominantly occurs within the $MoSe_2$ and WSe_2 layers, accompanied by a corresponding accumulation of charge on α-$RuCl_3$ and MoO_3. Other heterostructures, for example, $MoSe_2/MoO_3$ and WSe_2/α-$RuCl_3$, exhibit qualitatively similar features (see SI).

Though here we study the intrinsic charge transfer between pristine materials, we note that the application of an external electric field could be used to accentuate the band offset between the channel and the doping layer to increase the effectiveness of the modulation doping approach. We provide additional discussion of the pros and cons of external electric fields in the SI.

In Fig. 3 we provide the theoretical ionization potentials (E_{IP}) and electron affinities (E_{EA}) for a selection of different channel materials and doping layers. We considered seven 2D channel materials, all experimentally relevant for 2D semiconductor FETs, namely the transition-metal dichalcogenides, MoS_2, WSe_2, $MoSe_2$, and MoSSe, as well as 2D hexagonal AlN, BN, and GaN. These 2D channel materials are arranged in ascending order of the VBM relative to the vacuum level (corresponding to decreasing E_{IP}). WSe_2 exhibits the lowest ionization potential, $E_{IP} = 4.99$ eV, making it the most suitable candidate for type-III band alignment. Conversely, h-BN has its VBM situated far from the vacuum level, $E_{IP} = 6.61$ eV, which complicates the search for appropriate dopants.

Because chemical stability and interface compatibility are important considerations for choosing p-type dopant materials, we studied a wide range of stable 2D or layered materials as potential charge transfer layers, including many binary transition metal oxides, as well as α-$RuCl_3$, oxyhalides, and perovskite layers. Fig. 3(a) shows the successful combinations of channel and doping layers for which the theoretically predicted band alignment makes p-doping of WSe_2 possible. In Fig. 3(b) we also show the *unsuccessful* combinations of materials, where the doping layer does *not* exhibit a type-III band alignment with any of the investigated 2D channels. Below we provide a summary of the various charge transfer layers and highlight relevant materials based on their IPs and EAs.

We begin with α-$RuCl_3$, which is known to significantly hole-dope graphene and WSe_2 [3, 17]. This narrow-band Mott insulator exhibits a notably large work function, $E_{EA} = 6.1$ eV (see Fig. 3), which significantly surpasses the typical work functions of common layered materials such as graphene ($E_{IP} = 4.6$ eV) and WSe_2 ($E_{IP} = 4.4$ eV). The CBM of α-$RuCl_3$ is far away from the vacuum level, suggesting its potential applicability as an electron acceptor not only for graphene and WSe_2, but potentially for a wider range of 2D materials, particularly all of the 2D TMD channel materials and group III nitrides we considered except for BN. This combination of a large work function and deep CBM distinguishes α-$RuCl_3$ as a important material within this context.

High electron affinity transition metal oxides, such as molybdenum trioxide (AA MoO_3, $E_{EA} = 6.4$ eV), tungsten trioxide (WO_3, $E_{EA} = 6.4$ eV), and vanadium pentoxide (V_2O_5, $E_{EA} = 6.46$ eV), are well-established and highly effective surface acceptors [34, 35]. MoO_3 exhibits various phases that have been studied under different synthesis conditions. These phases include the thermodynamically stable and most well studied α-MoO_3 (AA)

and several metastable forms such as II-MoO_3 (AB), h-MoO_3, and β-MoO_3. The fundamental structure of MoO_3 is based on MoO_6 octahedra, where a central molybdenum atom is surrounded by six oxygen atoms. The electronic structure of bulk MoO_3 surfaces and interfaces with organic semiconductors has been studied theoretically using DFT calculations, but its effect on the energy band levels of diverse 2D channel materials for FET applications remains an open question. Our study highlights stable α-MoO_3, as well as metastable II-MoO_3, h-MoO_3, and β-MoO_3, as promising candidates for modulating the electronic properties of all the 2D channel materials we investigated. While current FET literature primarily focuses on doping WSe_2 with MoO_3, our findings suggest exciting new avenues for doping other materials, including hBN, AlN, GaN, and MoS_2 — a prospect that warrants further investigation. α-MoO_3 facilitates spontaneous electron transfer from WSe_2 to itself, effectively injecting holes into the WSe_2 layer in agreement with the band alignment presented in Fig. 3 [36]. WO_3 shares the same basic structure with MoO_3 and has an electron affinity of 6.4 eV, making it also a promising candidate for type-III band alignment (see Fig. 3) [37].

The prevalent α phase of V_2O_5, characterized by the Pmnm space group, features a structure where single layers consist of edge- and corner-sharing square pyramids, with adjacent layers bound together along the c-axis through weak vdW interactions. Notably, V_2O_5 boasts a layered structure, a direct band gap within the visible-light region, and impressive chemical and thermal stability. This material is easy to prepare and has been used in heterostructure engineering with graphene and MXenes to enhance cathode performance [38]. V_2O_5 has an extremely high electron affinity (6.46 eV), which makes it suitable for hole doping in six of the seven 2D materials evaluated in this study (see Fig. 3).

The crystal structure of chromium trioxide (CrO_3) consists of chromium atoms surrounded by a tetrahedron of four oxygen atoms. The corner-sharing tetrahedra form a chain-like arrangement, wherein each Cr atom shares two O atoms with its adjacent Cr atoms along the chain. CrO_3 has an extremely high electron affinity (6.75 eV) suitable for hole doping all seven 2D channel materials evaluated (see Fig. 3).

Layered Ga_2O_3 exhibits a type-III band alignment in Ga_2O_3/SiC vdW heterostructures [39], and our calculations show that it will likely p-dope WSe_2 and possibly $MoSe_2$. We also predict p-type doping of WSe_2 using Ta_2O_5, which is stable in an orthorhombic phase. Monolayer GeO_2 warrants consideration as well. Its extremely wide excitonic gap of 6.24 eV [40], positions it differently compared to the other materials investigated. This substantial bandgap, coupled with a relatively high work function (E_{EA} = 5 eV) offer distinctive charge transfer characteristics. The successful fabrication of 2D GeO_2 further motivates its exploration [41].

Even among the potential charge transfer layer combinations that do not exhibit type-III band alignment, shown in Fig. 3(b), several are worth noting. Monolayers of the form A_2BO_4 are derived from cubic perovskites (ABO_3) and can be thought of as a single layer of the Ruddlesden-Popper phase with $n = 1$ [42]. Though they cannot serve as charge transfer layers for any of the considered 2D channel materials, since the energy of their valence bands is comparable to that of WSe_2 they could potentially be p-doped themselves by many of the binary oxides we studied. The oxyhalides BiBrO and BiClO, which possess extremely high electron affinities [43, 44], are also interesting. Their bands are not far from type-III alignment with WSe_2 and $MoSe_2$, suggesting they may serve as potential p-type dopants, especially if defects or other surface details tip the balance in their favor.

III. SUMMARY AND CONCLUSIONS

The main results of this study are contained in Fig. 3: part (a) showcases many promising candidates for p-type doping of 2D materials, all warranting further exploration and experimental validation; conversely, part (b) identifies candidate combinations that are not likely to work. Our systematic investigation of band alignments of 27 materials including oxides, oxyhalides, and α-$RuCl_3$, with respect to TMDs and III-nitrides, provides a comprehensive foundation for future explorations of vdW heterostructures with optimized interfacial electronic properties for advanced electronic and optoelectronic devices.

Moreover, our study motivates a broader investigation into the doping capabilities of sub-stoichiometric metal oxides beyond the commonly explored MoO_x, AlO_x, and TiO_x [11, 45]. The non-stoichiometry in these oxides can introduce vacancies and alter the electronic structure, showing great promise as dopants. Expanding the exploration of such materials could unlock new avenues for fine-tuning the electronic properties of 2D materials.

The electronic behavior of the interfaces between the materials studied here can be significantly influenced by a range of physical phenomena. These include the orientation and termination of the oxide surface, the presence of localized defects, and stress-induced band distortions. Thermal stress poses a challenge to the stability of interfacial charge transfer, as highlighted by studies on perovskite solar cells [46, 47]. At elevated temperatures, diffusion or migration of atoms across the interface can occur, potentially altering the electronic landscape and degrading performance [48, 49].
Moreover, repeated thermal cycling—a common condition in electronic applications—can induce mechanical stress. This stress may lead to changes in the phases or structures of materials, affecting their ability to facilitate charge transfer. A study investigating the effect of rapid cyclic thermal stress on TMD FETs found that while an Al_2O_3 passivation layer initially improved device charac-

teristics, prolonged cycling led to permanent interfacial damage, increasing trap density and altering hysteresis behavior[50]. Chemical stability is also important, since oxidation and humidity can degrade components in a heterostructure and weaken charge transfer pathways, reducing device efficiency [51]. While MoO_3 and V_2O_5 are noted for their robustness against common environmental factors, their reaction to thermal stress remains crucial for reliable operation [52]. ~~Furthermore, calculations of band energies with respect to the vacuum level can be sensitive to the choice of exchange-correlation functional.~~ A comprehensive exploration of all these processes should be the subject of future work for more detailed predictions.

A. Methods

We performed first-principles density functional theory (DFT) calculations using the Vienna Ab initio Simulation Package (VASP) code [53]. The interactions between valence electrons and ionic cores were described using the projector augmented-wave (PAW) method [54]. To model the exchange-correlation interactions among electrons, we employed two complementary approaches: the generalized gradient approximation (GGA) with the Perdew-Burke-Ernzerhof (PBE) functional [55], and the screened hybrid functional HSE06 [56] with default parameters. The HSE06 functional incorporates a fraction of exact Hartree-Fock exchange, effectively mitigating the band gap underestimation commonly observed in standard GGA calculations.

To ensure the accuracy of our calculations, we systematically tested convergence with respect to the plane-wave energy cutoff and k-point mesh density for each material. Structural optimizations were meticulously performed using the conjugate-gradient algorithm, allowing full relaxation of both unit cell parameters and internal atomic positions until residual forces were less than 0.001 eV/Å. We introduced a vacuum spacing of 18 Å along the direction perpendicular to the surface to eliminate spurious interactions between periodically repeated images. Furthermore, we accounted for long-range van der Waals interactions using the DFT-D2 method of Grimme [57], which adds a semi-empirical dispersion correction to the standard DFT energy. Optimized structural parameters are detailed in Table S1 of the Supporting Information. Subsequently, we performed highly converged self-consistent field (SCF) calculations using denser k-point grids than those used during structural optimization to ensure an accurate determination of electronic properties.

Accurately determining ionization potentials (IPs) and electron affinities (EAs) for solid-state systems is challenging due to the influence of surface dipoles. We, therefore, employed a two-step computational approach. First, we performed calculations on bulk models to determine the energy levels of the valence band maximum (VBM) and conduction band minimum (CBM) relative to a common reference energy level. Next, we constructed surface slab models with appropriate terminations and sufficient vacuum spacing to simulate the material-vacuum interface. Calculations on these slabs yielded the electrostatic potential difference between the vacuum level and the reference level established in the bulk calculations, intrinsically capturing the surface dipole contribution [24, 58]. By aligning the reference levels from both calculations, we accurately computed the IPs and EAs. Finally, the work function, a key property governing electron emission, was directly calculated as the difference between the vacuum level potential and the Fermi level, extracted from the electrostatic potential profile of the relaxed surface slab models.

For the heterostructures with TMD monolayer and monolayer α-$RuCl_3$, we used a hexagonal supercell composed of a 4×4 TMD supercell and 2×2 α-$RuCl_3$ supercell. The geometric structure of heterostructures are relaxed by fixing TMD layers to the $RuCl_3$ lattice constant (6.02 Å) with fully relaxed force of $RuCl_3$. A rectangular supercell of (Mo/W)Se_2 (4×2×1) and MoO_3 (3×3×1) are used to reduce the stress induced by the lattice mismatch between materials while balancing the computational burden. The geometric structure of heterostructures are relaxed by fixing TMD layers to the MoO_3 lattice constant (a = 3.68 Åand b = 3.91 Å) with fully relaxed force of MoO_3.

ACKNOWLEDGEMENT

The authors thank Tomas Palacios, Jing Kong, Jagadeesh Moodera and their research groups for valuable discussions. This work was supported mainly by Army Research Office Agreement Number W911NF-23-2-0057, and partly by ARO Agreement Number W911NF-21-1-0184 and ARO Cooperative Agreement Number W911NF-21-2-0147. Calculations were performed on the FASRC cluster supported by the FAS Division of Science Research Computing Group at Harvard University.

SUPPLEMENTARY INFORMATION

The Supplementary Information contains technical details and parameters of first-principles calculations, ~~along with~~ additional results of the structural and electronic properties, and ~~related systems~~ further discussion of the effects of external electric fields on interfacial charge transfer.

[1] A. Chaves, J. G. Azadani, H. Alsalman, D. Da Costa, R. Frisenda, A. Chaves, S. H. Song, Y. D. Kim, D. He, J. Zhou, *et al.*, Bandgap engineering of two-dimensional semiconductor materials, npj 2D Materials and Applications **4**, 29 (2020).

[2] K. S. Novoselov, A. Mishchenko, A. Carvalho, and A. Castro Neto, 2D materials and van der Waals heterostructures, Science **353**, aac9439 (2016).

[3] J. Xie, Z. Zhang, H. Zhang, V. Nagarajan, W. Zhao, H.-L. Kim, C. Sanborn, R. Qi, S. Chen, S. Kahn, *et al.*, Low resistance contact to p-type monolayer WSe_2, Nano Letters **24**, 5937 (2024).

[4] R. Wu, H. Zhang, H. Ma, B. Zhao, W. Li, Y. Chen, J. Liu, J. Liang, Q. Qin, W. Qi, *et al.*, Synthesis, modulation, and application of two-dimensional tmd heterostructures, Chemical Reviews (2024).

[5] D. Akinwande, C. Huyghebaert, C.-H. Wang, M. I. Serna, S. Goossens, L.-J. Li, H.-S. P. Wong, and F. H. Koppens, Graphene and two-dimensional materials for silicon technology, Nature **573**, 507 (2019).

[6] B. Radisavljevic, A. Radenovic, J. Brivio, V. Giacometti, and A. Kis, Single-layer MoS_2 transistors, Nature nanotechnology **6**, 147 (2011).

[7] V. K. Sangwan, H.-S. Lee, H. Bergeron, I. Balla, M. E. Beck, K.-S. Chen, and M. C. Hersam, Multi-terminal memtransistors from polycrystalline monolayer molybdenum disulfide, Nature **554**, 500 (2018).

[8] Y. Wu, D. Li, C.-L. Wu, H. Y. Hwang, and Y. Cui, Electrostatic gating and intercalation in 2D materials, Nature Reviews Materials **8**, 41 (2023).

[9] Y. Wang, J. C. Kim, Y. Li, K. Y. Ma, S. Hong, M. Kim, H. S. Shin, H. Y. Jeong, and M. Chhowalla, P-type electrical contacts for 2D transition-metal dichalcogenides, Nature **610**, 61 (2022).

[10] N. H. Patoary, J. Xie, G. Zhou, F. Al Mamun, M. Sayyad, S. Tongay, and I. S. Esqueda, Improvements in 2D p-type WSe_2 transistors towards ultimate CMOS scaling, Scientific reports **13**, 3304 (2023).

[11] C. J. McClellan, E. Yalon, K. K. Smithe, S. V. Suryavanshi, and E. Pop, High current density in monolayer MoS_2 doped by AlO_x, ACS nano **15**, 1587 (2021).

[12] S.-Y. Seo, G. Moon, O. F. Okello, M. Y. Park, C. Han, S. Cha, H. Choi, H. W. Yeom, S.-Y. Choi, J. Park, *et al.*, Reconfigurable photo-induced doping of two-dimensional van der Waals semiconductors using different photon energies, Nature Electronics **4**, 38 (2021).

[13] D. Wang, X.-B. Li, and H.-B. Sun, Modulation doping: a strategy for 2D materials electronics, Nano Letters **21**, 6298 (2021).

[14] P.-H. Ho, J.-R. Chang, C.-H. Chen, C.-H. Hou, C.-H. Chiang, M.-C. Shih, H.-C. Hsu, W.-H. Chang, J.-J. Shyue, Y.-P. Chiu, *et al.*, Hysteresis-free contact doping for high-performance two-dimensional electronics, ACS nano **17**, 2653 (2023).

[15] G. Shao, Work function and electron affinity of semiconductors: Doping effect and complication due to fermi level pinning, Energy & Environmental Materials **4**, 273 (2021).

[16] D. Lee, J. J. Lee, Y. S. Kim, Y. H. Kim, J. C. Kim, W. Huh, J. Lee, S. Park, H. Y. Jeong, Y. D. Kim, *et al.*, Remote modulation doping in van der Waals heterostructure transistors, Nature Electronics **4**, 664 (2021).

[17] Y. Wang, J. Balgley, E. Gerber, M. Gray, N. Kumar, X. Lu, J.-Q. Yan, A. Fereidouni, R. Basnet, S. J. Yun, *et al.*, Modulation doping via a two-dimensional atomic crystalline acceptor, Nano letters **20**, 8446 (2020).

[18] V. O. Özçelik, J. G. Azadani, C. Yang, S. J. Koester, and T. Low, Band alignment of two-dimensional semiconductors for designing heterostructures with momentum space matching, Physical Review B **94**, 035125 (2016).

[19] J. Ristein, Surface transfer doping of semiconductors, Science **313**, 1057 (2006).

[20] S. Lu, P. Shen, H. Zhang, G. Liu, B. Guo, Y. Cai, H. Chen, F. Xu, T. Zheng, F. Xu, *et al.*, Towards n-type conductivity in hexagonal boron nitride, Nature Communications **13**, 3109 (2022).

[21] Y. Wang, S. Sarkar, H. Yan, and M. Chhowalla, Critical challenges in the development of electronics based on two-dimensional transition metal dichalcogenides, Nature Electronics , 1 (2024).

[22] K. G. Crawford, D. Qi, J. McGlynn, T. G. Ivanov, P. B. Shah, J. Weil, A. Tallaire, A. Y. Ganin, and D. A. Moran, Thermally stable, high performance transfer doping of diamond using transition metal oxides, Scientific Reports **8**, 3342 (2018).

[23] A. Kuruvila, P. R. Kidambi, J. Kling, J. B. Wagner, J. Robertson, S. Hofmann, and J. Meyer, Organic light emitting diodes with environmentally and thermally stable doped graphene electrodes, Journal of Materials Chemistry C **2**, 6940 (2014).

[24] K. T. Butler, R. Crespo-Otero, J. Buckeridge, D. O. Scanlon, E. Bovill, D. Lidzey, and A. Walsh, Band energy control of molybdenum oxide by surface hydration, Applied Physics Letters **107** (2015).

[25] J. Meyer, P. R. Kidambi, B. C. Bayer, C. Weijtens, A. Kuhn, A. Centeno, A. Pesquera, A. Zurutuza, J. Robertson, and S. Hofmann, Metal oxide induced charge transfer doping and band alignment of graphene electrodes for efficient organic light emitting diodes, Scientific reports **4**, 5380 (2014).

[26] M. T. Greiner, M. G. Helander, W.-M. Tang, Z.-B. Wang, J. Qiu, and Z.-H. Lu, Universal energy-level alignment of molecules on metal oxides, Nature materials **11**, 76 (2012).

[27] M. T. Greiner and Z.-H. Lu, Thin-film metal oxides in organic semiconductor devices: their electronic structures, work functions and interfaces, NPG Asia Materials **5**, e55 (2013).

[28] C. Lei, Y. Ma, X. Xu, T. Zhang, B. Huang, and Y. Dai, Broken-gap type-III band alignment in WTe_2/HfS_2 van der Waals heterostructure, The Journal of Physical Chemistry C **123**, 23089 (2019).

[29] C.-W. Yang, H.-L. Tang, S. Sattar, M.-H. Chiu, Y. Wan, C.-H. Chen, J. Kong, K.-W. Huang, L.-J. Li, and V. Tung, Epitaxial growth and determination of band alignment of Bi_2Te_3–WSe_2 vertical van der Waals heterojunctions, ACS Materials Letters **2**, 1351 (2020).

[30] S. Zhao, C. Yang, Z. Zhu, X. Yao, and W. Li, Curvature-controlled band alignment transition in 1D van der Waals heterostructures, npj Computational Materials **9**, 92 (2023).

[31] D. Guo, Q. Fu, G. Zhang, Y. Cui, K. Liu, X. Zhang, Y. Yu, W. Zhao, T. Zheng, H. Long, *et al.*, Composition modulation-mediated band alignment engineering from type I to type III in 2D vdW heterostructures, Advanced Materials , 2400060 (2024).

[32] J. Pack, Y. Guo, Z. Liu, B. S. Jessen, L. Holtzman, S. Liu, M. Cothrine, K. Watanabe, T. Taniguchi, D. G. Mandrus, *et al.*, Charge-transfer contacts for the measurement of correlated states in high-mobility WSe_2, Nature Nanotechnology , 1 (2024).

[33] Y. Cho, G. R. Schleder, D. T. Larson, E. Brutschea, K.-E. Byun, H. Park, P. Kim, and E. Kaxiras, Modulation doping of single-layer semiconductors for improved contact at metal interfaces, Nano Letters **22**, 9700 (2022).

[34] J. Yun, W. Jang, T. Lee, Y. Lee, and A. Soon, Aligning the band structures of polymorphic molybdenum oxides and organic emitters in light-emitting diodes, Physical Review Applied **7**, 024025 (2017).

[35] P. Hu, P. Hu, T. D. Vu, M. Li, S. Wang, Y. Ke, X. Zeng, L. Mai, and Y. Long, Vanadium oxide: phase diagrams, structures, synthesis, and applications, Chemical Reviews **123**, 4353 (2023).

[36] L. Cai, C. J. McClellan, A. L. Koh, H. Li, E. Yalon, E. Pop, and X. Zheng, Rapid flame synthesis of atomically thin moo3 down to monolayer thickness for effective hole doping of WSe_2, Nano letters **17**, 3854 (2017).

[37] F. Wang, C. Di Valentin, and G. Pacchioni, Electronic and structural properties of WO_3: a systematic hybrid dft study, The Journal of Physical Chemistry C **115**, 8345 (2011).

[38] P. Falun, L. Ngamwongwan, S. Singsen, M. Chotsawat, P. Komen, A. Junkaew, and S. Suthirakun, Enhancing v2o5 cathode performance through heterostructure engineering with the $Ti_3C_2O_2$ MXene: A computational study, The Journal of Physical Chemistry C (2024).

[39] N. Ferdous, M. S. Islam, and J. Park, A resilient type-III broken gap Ga_2O_3/SiC van der Waals heterogeneous bilayer with band-to-band tunneling effect and tunable electronic property, Scientific Reports **14**, 12748 (2024).

[40] Y. Sozen, M. Yagmurcukardes, and H. Sahin, Vibrational and optical identification of GeO_2 and GeO single layers: a first-principles study, Physical Chemistry Chemical Physics **23**, 21307 (2021).

[41] B. Y. Zhang, K. Xu, Q. Yao, A. Jannat, G. Ren, M. R. Field, X. Wen, C. Zhou, A. Zavabeti, and J. Z. Ou, Hexagonal metal oxide monolayers derived from the metal–gas interface, Nature Materials **20**, 1073 (2021).

[42] S. Ruddlesden and P. Popper, The compound $Sr_3Ti_2O_7$ and its structure, Acta Crystallogr. **11**, 54 (1958).

[43] Z. Ran, X. Wang, Y. Li, D. Yang, X.-G. Zhao, K. Biswas, D. J. Singh, and L. Zhang, Bismuth and antimony-based oxyhalides and chalcohalides as potential optoelectronic materials, npj Computational Materials **4**, 14 (2018).

[44] M. D. Prasad, G. V. Ramesh, and S. K. Batabyal, 2D layered structure of bismuth oxyhalides for advanced applications, in *Adapting 2D Nanomaterials for Advanced Applications* (ACS Publications, 2020) pp. 295–315.

[45] M. Shahrokhi, P. Raybaud, and T. Le Bahers, 2D $MoO_{3-x}S_x/MoS_2$ van der Waals assembly: a tunable heterojunction with attractive properties for photocatalysis, ACS applied materials & interfaces **13**, 36465 (2021).

[46] A. D. Sheikh, R. Munir, M. A. Haque, A. Bera, W. Hu, P. Shaikh, A. Amassian, and T. Wu, Effects of high temperature and thermal cycling on the performance of perovskite solar cells: acceleration of charge recombination and deterioration of charge extraction, ACS applied materials & interfaces **9**, 35018 (2017).

[47] Q. Zhou, B. Wang, R. Meng, J. Zhou, S. Xie, X. Zhang, J. Wang, S. Yue, B. Qin, H. Zhou, *et al.*, Understanding temperature-dependent charge extraction and trapping in perovskite solar cells, Advanced Functional Materials **30**, 2000550 (2020).

[48] Z. Dai, N. Lu, K. M. Liechti, and R. Huang, Mechanics at the interfaces of 2d materials: Challenges and opportunities, Current Opinion in Solid State and Materials Science **24**, 100837 (2020).

[49] J. M. Polfus, M. B. Muñiz, A. Ali, D. A. Barragan-Yani, P. E. Vullum, M. F. Sunding, T. Taniguchi, K. Watanabe, and B. D. Belle, Temperature-dependent adhesion in van der waals heterostructures, Advanced Materials Interfaces **8**, 2100838 (2021).

[50] Y. Kim, B. Kaczer, D. Verreck, A. Grill, D. Kim, J. Song, J. Diaz-Fortuny, A. Vici, J. Park, S. Van Beek, *et al.*, Cyclic thermal effects on devices of two-dimensional layered semiconducting materials, Advanced Electronic Materials **7**, 2100348 (2021).

[51] Q. Li, Q. Zhou, L. Shi, Q. Chen, and J. Wang, Recent advances in oxidation and degradation mechanisms of ultrathin 2d materials under ambient conditions and their passivation strategies, Journal of Materials Chemistry A **7**, 4291 (2019).

[52] J. Moura, J. Silveira, J. da Silva Filho, A. Souza Filho, C. Luz-Lima, and P. Freire, Temperature-induced phase transition in h-MoO_3: Stability loss mechanism uncovered by raman spectroscopy and dft calculations, Vibrational Spectroscopy **98**, 98 (2018).

[53] G. Kresse and J. Furthmüller, Efficiency of ab-initio total energy calculations for metals and semiconductors using a plane-wave basis set, Computational materials science **6**, 15 (1996).

[54] P. E. Blöchl, Projector augmented-wave method, Physical review B **50**, 17953 (1994).

[55] J. P. Perdew, K. Burke, and M. Ernzerhof, Generalized gradient approximation made simple, Physical review letters **77**, 3865 (1996).

[56] J. Heyd, G. E. Scuseria, and M. Ernzerhof, Hybrid functionals based on a screened coulomb potential, The Journal of chemical physics **118**, 8207 (2003).

[57] S. Grimme, Semiempirical gga-type density functional constructed with a long-range dispersion correction, Journal of computational chemistry **27**, 1787 (2006).

[58] S. Kiyohara, Y. Hinuma, and F. Oba, Band alignment of oxides by learnable structural-descriptor-aided neural network and transfer learning, Journal of the American Chemical Society **146**, 9697 (2024).

[59] S. Wang, H. Tian, C. Ren, J. Yu, and M. Sun, Electronic and optical properties of heterostructures based on transition metal dichalcogenides and graphene-like zinc oxide, Scientific reports **8**, 12009 (2018).

[60] E. Yang, S. Hong, J. Ma, S.-J. Park, D. K. Lee, T. Das, T.-J. Ha, J. Y. Kwak, and J. Chang, Realization of extremely high-gain and low-power in nmos inverter based on monolayer WS_2 transistor operating in subthreshold regime, ACS nano (2024).

[61] Supplemental Material, See Supplemental Material at URL provided by the publisher for technical details and parameters of first-principles calculations. The Supple-

mental Material also contains Refs. [62-70].

[62] L. Xu, W.-Q. Huang, W. Hu, K. Yang, B.-X. Zhou, A. Pan, and G.-F. Huang, Two-dimensional MoS_2-graphene-based multilayer van der waals heterostructures: enhanced charge transfer and optical absorption, and electric-field tunable dirac point and band gap, Chemistry of Materials **29**, 5504 (2017).

[63] H. Schmidt, F. Giustiniano, and G. Eda, Electronic transport properties of transition metal dichalcogenide field-effect devices: surface and interface effects, Chemical Society Reviews **44**, 7715 (2015).

[64] S. Jiang, J. Shan, and K. F. Mak, Electric-field switching of two-dimensional van der waals magnets, Nature materials **17**, 406 (2018).

[65] W. Zan, W. Geng, H. Liu, and X. Yao, Electric-field and strain-tunable electronic properties of MoS_2/h-bn/graphene vertical heterostructures, Physical Chemistry Chemical Physics **18**, 3159 (2016).

[66] W. Li, T. Wang, X. Dai, X. Wang, C. Zhai, Y. Ma, S. Chang, and Y. Tang, Electric field modulation of the band structure in MoS_2/WS_2 van der waals heterostructure, Solid State Communications **250**, 9 (2017).

[67] K. Iordanidou, R. Mitra, N. Shetty, S. Lara-Avila, S. Dash, S. Kubatkin, and J. Wiktor, Electric field and strain tuning of 2d semiconductor van der waals heterostructures for tunnel field-effect transistors, ACS Applied Materials & Interfaces **15**, 1762 (2022).

[68] X. Lu, L. Li, X. Guo, J. Ren, H. Xue, and F. Tang, Effects of vertical strain and electric field on the electronic properties and interface contact of graphene/inp vdw heterostructure, Computational Materials Science **198**, 110677 (2021).

[69] T. Henderson, Model for degradation of gaas/algaas hbts under temperature and current stress, in *Proceedings of International Electron Devices Meeting* (IEEE, 1995) pp. 811–814.

[70] J. Pak, Y. Jang, J. Byun, K. Cho, T.-Y. Kim, J.-K. Kim, B. Y. Choi, J. Shin, Y. Hong, S. Chung, *et al.*, Two-dimensional thickness-dependent avalanche breakdown phenomena in MoS_2 field-effect transistors under high electric fields, ACS nano **12**, 7109 (2018).

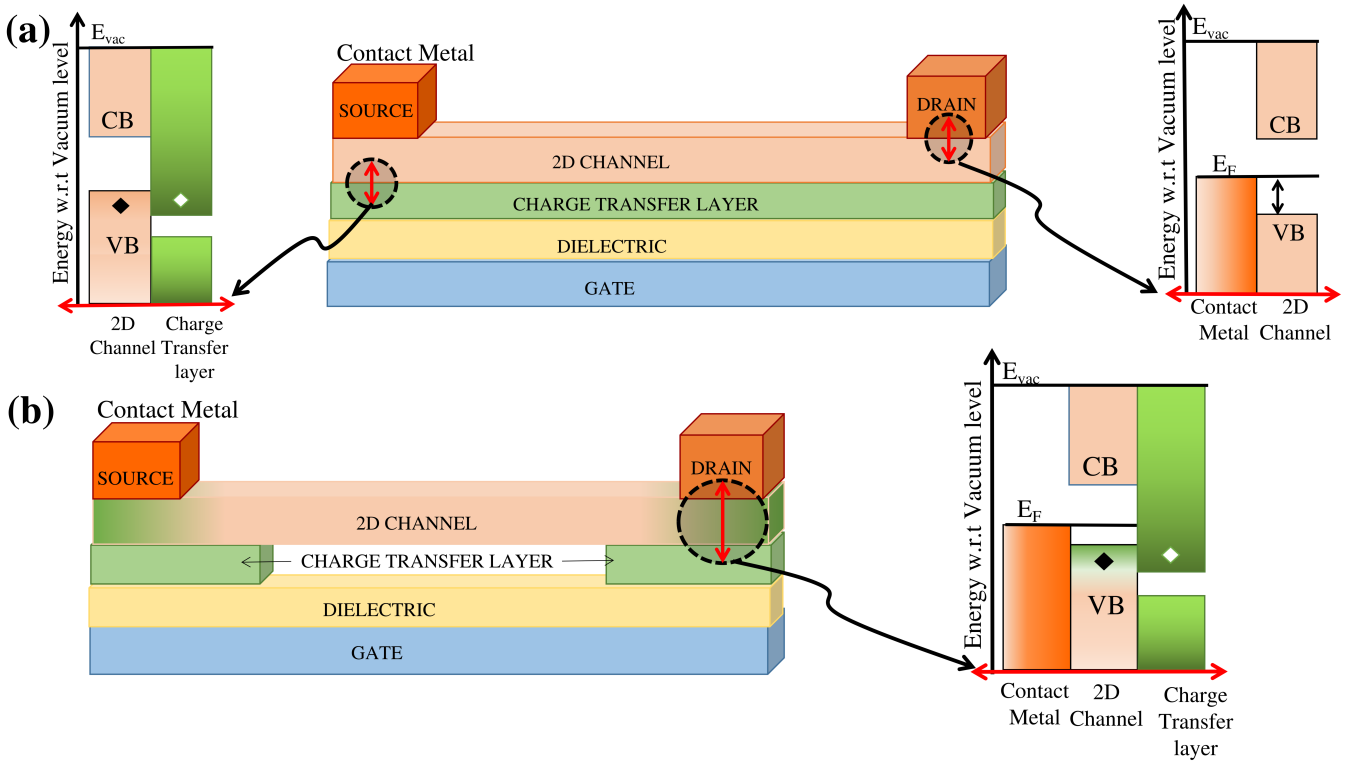


FIG. 1. Schematic device structure and electronic bands for modulation doping: (a) Source, drain, channel, and charge transfer layer (CTL) of a 2D-channel-based transistor. The band diagrams on each side illustrate the separate interfaces channel/CTL and drain/2D-channel. The difference in work function between the channel and CTL modifies the electronic bands, resulting in the charge transfer layer acting as a so-called 'van der Waals' electron acceptor, while the channel becomes significantly hole-doped after transferring its electrons. (b) Device with CTL localized near the contact, creating regions in the channel that are highly hole-doped. The band diagram on the right illustrates the expected charge redistribution when the channel and charge transfer layers are brought into contact. The modification of the channel work function serves to reduce the Schottky barrier.

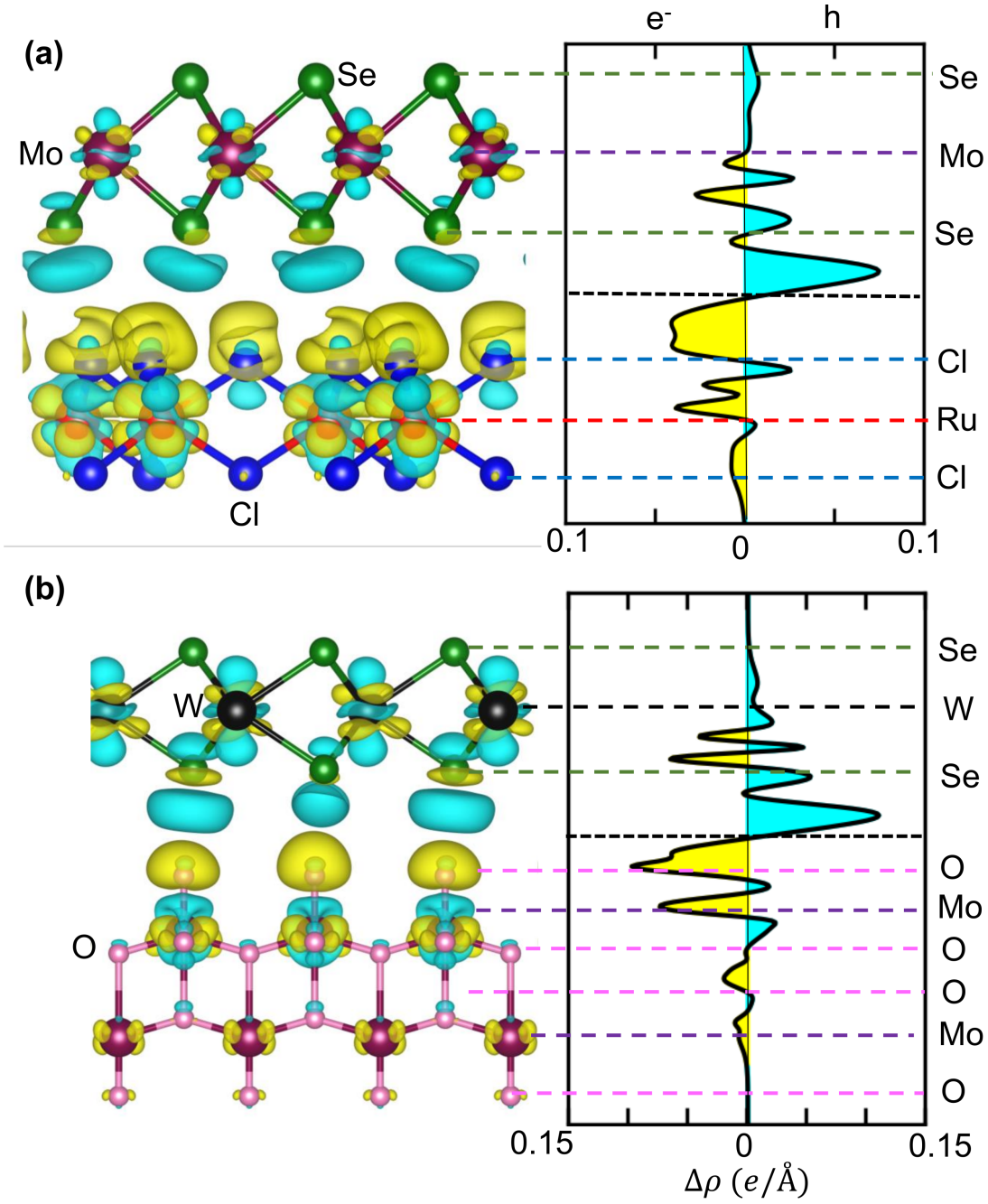


FIG. 2. Structures and isosurfaces of charge density difference between the combined hetrostructure and its constituent layers, for: (a) $MoSe_2$ and α-$RuCl_3$; (b) WSe_2 and MoO_3. Yellow contours show regions of electronic charge accumulation (extra electrons) and cyan contours indicate charge depletion (holes), demonstrating an overall transfer of electrons from the 2D channel to the charge transfer layer. Plots show the charge density difference averaged over horizontal planes as a function of the perpendicular (vertical) distance.

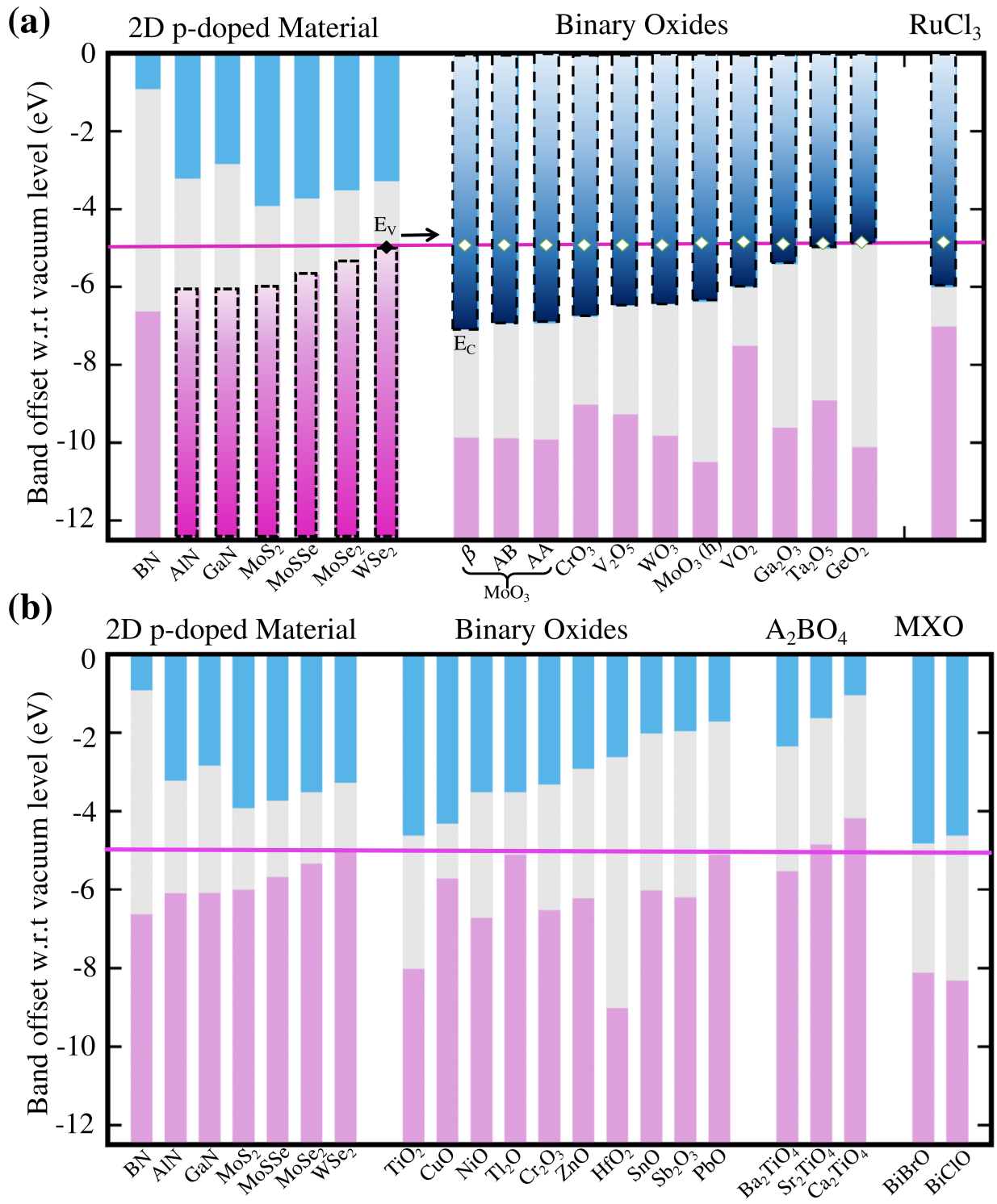


FIG. 3. (a) Band Alignments for p-Type Doping in 2D Materials. Valence and conduction band positions are shown with respect to the vacuum level for various 2D channel materials (left) and binary oxides acting as acceptor layers. The horizontal pink line, aligned with the VBM of WSe_2, highlights favorable type-III band alignments for p-type doping. Solid diamonds and black dashed lines indicate spontaneous charge transfer between WSe_2 and the suitable oxides. α-$RuCl_3$ also acts as an effective electron acceptor for all channel materials but hBN. (b) Band Alignments Lacking Type-III Character. VBM and CBM positions, referenced to the vacuum level, for binary oxides, A_2BO_4 pervoskite monolayers and MXOxides (M: metal, X: halide) that do not exhibit a type-III band alignment with the considered channel materials.